A MULTIFRACTAL LEVEL SET ALGORITHM FOR SEGMENTING HUMAN SKIN ULTRASOUND IMAGES

Meriem DJEDDI, Hadj BATATIA

University of Toulouse, IRIT/INPT
2, rue Charles Camichel 31071 Toulouse Cedex 7, France

ABSTRACT

Segmenting ultrasound images is a difficult task due to low contrast and speckle. Gradient based deformable models and classic region based active contours fail to correctly delineate biological structures. This paper goes beyond existing global and local statistics based models by proposing an active contour founded on multifractal properties. It consists of minimizing an energy functional based on the quadratic form of the log normal multiplicative cascade scaling law. The associated Euler equation is derived using shape derivation. A level-set method is used to solve the resulting partial derivative evolution equation. The algorithm is successfully applied to synthetic and real data. Results show that the method can be used to automatically delineate skin melanoma regions.

Index Terms— Multifractal, Segmentation, Active Contour, Multiplicative Cascade, Ultrasound images.

1. INTRODUCTION

Ultrasound medical imaging is an affordable and non invasive modality that has multiple clinical applications. Its recent technical developments make it a valid approach to assess skin tumors. However, its clinical exploitation in dermatology requires robust image processing algorithms to overcome their complex nature, especially due to speckle. Several segmentation techniques have been proposed in the literature to deal with this modality [21]. Methods based on active contours have received a great deal of investigations [20]. The use of global parametric statistics in active contours has started in [4] with Gaussian distribution, Rayleigh in [25], and generalized to the exponential distributions family in [15, 22]. Non parametric statics have also been used first in [13] and since then in various works (see [23, 29] and references therein). These approches have difficulty taking into consideration the local heterogeneous nature of speckle images. Local parametric statistics were introduced in [5,14] to deal with heterogeneity and used in [11,17,18] among others. The rational for using such models stems from the fact that local region statics relax the strong constraint of i.i.d. pixels in global statics. However these techniques are very sensitive to noise. Another way of dealing with the limitations of global statics consists of using non-local active contours [12, 19]. Joint local and global statistics have been combined in [26,27]. These works pose the problem of local scale selection that has been tackled in [2, 3, 24]. In this paper, we propose a model that, in a sense, unifies the use of global and local statics while dealing implicitly with the selection of the optimal spatial scale. This is achieved by developing a region-based active contour whose energy functional depends on multifractal properties estimated using a multiresolution framework. The multifractal properties are derived from a multiplicative cascade stochastic model that captures the statistics of the pixels and their inherent dependency. Fractal properties have already been used for medical image segmentation and characterization outside of the active contours framework [1, 8, 9, 16, 30]. However, in [6] it has been reported that ultrasound signals backscattered from the skin exhibit characteristic multifractal properties. We have previously shown that these properties can be explained by a lognormal multiplicative cascade model [7]. This paper builds on this result, and develops a multifractal active contour that separates regions in high frequency ultrasound images based on the distance between their scaling functions.

The remainder of the paper is structured as follows. Section 2 formulates the segmentation problem. The proposed multifractal active contour is detailed in Section 3, where the multifractal energy functional is established and the associated Euler equation is derived following the shape derivation scheme developed in [10]. Experiments on simulated and real data are presented in Section 4. Conclusions are finally reported in Section 5.

2. PROBLEM STATEMENT

As mentioned above, it has been shown in [7] that the multiplicative cascade with log normal multipliers is an appropriate stochastic model to describe the scale invariance of ultrasound signals backscattered from skin tissues. This model has the important characteristics of incorporating both the statistical properties of pixels and their inherent dependency. Considering the $3D$ image as a piecewise constant multiplicative lognormal cascade stationary process, every $3D$ region R can be

978-0-9928626-3-3/15/$31.00 ©2015 IEEE

characterized by its speckle scaling function $\tau_{R}(q)$:

$$\tau_{R}(q) = \frac{\sigma_{R}^2}{2}q^2 - \mu_{R}q; \tau_{R}(0) = \tau_{R}(1) = 0 \quad (1)$$

with q the statistical order of the moments ($q \in [-2, 2]$) and μ_{R} and σ_{R} the mean and variance of the lognormal cascade multipliers for R. In this work, we aim at segmenting a lesion located within a region representing the skin dermis. Accordingly, we consider the partition of the ultrasound image domain Ω into Ω_{in} and Ω_{out} produced by a surface Γ. Each partition would have a speckle scaling function $\tau_{\Omega.}(q)$.

3. PROPOSED METHOD

High Frequency Ultrasound (HFUS) data can well be described by a log-normal multiplicative cascade stochastic model [7]. Following this model, a homogenous region R can be characterized by the parameters μ_{R} and σ_{R}^2:

$$\mu_{R} = h_0^{(R)}\log(2) \quad (2)$$

$$\sigma_{R}^2 = (h_{qmax}^{(R)} - h_{qmin}^{(R)})log(2) \quad (3)$$

where $h_q^{(R)}$ is the Holder exponent of order q for the region R. Following [28], $h_q^{(R)}$ can be directly estimated from multiple scale wavelet coefficients as follows:

$$h_q^{(R)} = \sum_{j=1}^{J}\omega_j \iiint_{R} \frac{T_j(x,y,z)^q log_2(T_j(x,y,z))}{\iiint_{R} T_j(x,y,z)^q dxdydz}dxdydz \quad (4)$$

where ω_j are weights estimated according to the regression method described in [28] and $T_j(x,y,z)$ is the wavelet coefficient at (x,y,z) for the scale j. For simplicity, $\mathbf{x}$ will denote the coordinates (x,y,z) and $d\mathbf{x}$ denotes $dxdydz$.

3.1. Energy functional

The segmentation problem is formulated as the search for the partition that maximizes the distance between $\tau_{\Omega_{in}}(q)$ and $\tau_{\Omega_{out}}(q)$. This distance is measured using the Earth Mover's Distance (EMD). The functional to optimize is:

$$J(\Omega) = \sum_{q=-2}^{2}|\tau_{\Omega_{in}}(q) - \tau_{\Omega_{out}}(q)| \quad (5)$$

By replacing eq.(4) in (2) and (3) and those in (5), and introducing a pseudo-time t, we obtain

$$J(\Omega,t) = \sum_{q=-2}^{2}\left|\sum_{j=1}^{J}\omega_j\left[\iiint_{\Omega_{out}(t)} k_{out}(\mathbf{x},q,j)d\mathbf{x} + \iiint_{\Omega_{in}(t)} k_{in}(\mathbf{x},q,j)d\mathbf{x}\right]\right|$$

where

$$k_{out}(\mathbf{x},q,j) = \frac{qlog(2)log_2(T_j(\mathbf{x}))}{\left[\iiint_{\Omega_{out}(t)} d\mathbf{x}\right]^2} - \frac{q^2log(2)T_j(\mathbf{x})^{qmax}log_2(T_j(\mathbf{x}))}{\iiint_{\Omega_{out}(t)} T_j(\mathbf{x})^{qmax}d\mathbf{x}} + \frac{q^2log(2)T_j(\mathbf{x})^{qmin}log_2(T_j(\mathbf{x}))}{\iiint_{\Omega_{out}(t)} T_j(\mathbf{x})^{qmin}d\mathbf{x}}$$

$$k_{in}(\mathbf{x},q,j) = -\frac{qlog(2)log_2(T_j(\mathbf{x}))}{\left[\iiint_{\Omega_{in}(t)} d\mathbf{x}\right]^2} + \frac{q^2log(2)T_j(\mathbf{x})^{qmax}log_2(T_j(\mathbf{x}))}{\iiint_{\Omega_{in}(t)} T_j(\mathbf{x})^{qmax}d\mathbf{x}} - \frac{q^2log(2)T_j(\mathbf{x})^{qmin}log_2(T_j(\mathbf{x}))}{\iiint_{\Omega_{in}(t)} T_j(\mathbf{x})^{qmin}d\mathbf{x}}$$

where $\iiint_{\Omega.(t)} d\mathbf{x}$ represents the number of pixels in the region $\Omega_{in}(t)$. Let $E(\Omega,q,j,t)$ be

$$E(\Omega,q,j,t) = \iiint_{\Omega_{out}(t)} k_{out}(\mathbf{x},q,j)d\mathbf{x} + \iiint_{\Omega_{in}(t)} k_{in}(\mathbf{x},q,j)d\mathbf{x}$$

The functional $E(\Omega,q,j,t)$ corresponds to the scale j and the order q. We can then write the global functional $J(\Omega,t)$ as a function of this inner functional $E(\Omega,q,j,t)$:

$$J(\Omega,t) = \sum_{q=-2}^{2}\left|\sum_{j=1}^{J}\omega_j\left[E(\Omega,q,j,t)\right]\right|. \quad (6)$$

3.2. Shape Derivation

In order to establish the evolution equation of the curve for this functional, we need to derive the expression of the flow by calculating the derivative $dJ(\Omega,t)/dt$. For this purpose, we are first interested in $dE(\Omega,q,j,t)/dt$. This term has the required form to allow the application of the shape derivation [1].

$$\frac{\partial E(\Omega,q,j,t)}{\partial t} = \int_{\Gamma(t)}\left[k_{out}(\mathbf{x},q,j,t) - k_{in}(\mathbf{x},q,j,t)\right](\vec{V}.\vec{N})ds + \iiint_{\Omega_{in}}\frac{\partial k_{in}(\mathbf{x},q,j,t)}{\partial t}d\mathbf{x} + \iiint_{\Omega_{out}(t)}\frac{\partial k_{out}(\mathbf{x},q,j,t)}{\partial t}d\mathbf{x} \quad (7)$$

where $\vec{V}$ is a vector field that defines the direction of the transformation of the domain depending on t and $\vec{N}$ is the normal to the curve Γ. Developing this derivative requires establishing the expressions of $\frac{\partial k_{in}}{\partial t}$ and $\frac{\partial k_{out}}{\partial t}$. For this purpose, we follow the shape derivation scheme presented in [10]. Accordingly, it can be shown that:

$$\iiint_{in}\frac{\partial k_{in}(\mathbf{x},j,q,t)}{\partial t} = \sum_{i=1}^{3}A_i^{(in)}\int_{\Gamma(t)}H_i^{(in)}(\mathbf{x},j)(\vec{V}.\vec{N})ds \quad (8)$$

where $H_i^{(in)}$ and $A_i^{(in)}$ are defined as:

$$H_1^{(in)}(\mathbf{x},j) = 1; \quad H_2^{(in)}(\mathbf{x},j) = T_j(\mathbf{x})^{qmax}; \quad H_3^{(in)}(\mathbf{x},j) = T_j(\mathbf{x})^{qmin}$$

[1] framework developed in [10], where $\vec{V}$ is the direction of the Eulerian derivative

$$A_1^{(\text{in})} = \iiint_{\Omega_{\text{in}}(t)} \frac{-qlog(2)log_2(T_j(\mathbf{x}))}{\left[G_1^{(\text{in})}(j,t)\right]^2} d\mathbf{x}$$

$$A_2^{(\text{in})} = \iiint_{\Omega_{\text{in}}(t)} \frac{\frac{q^2log(2)}{2} T_j(\mathbf{x})^{\text{qmax}} log_2(T_j(\mathbf{x}))}{\left[G_2^{(\text{in})}(j,t)\right]^2} d\mathbf{x}$$

$$A_3^{(\text{in})} = \iiint_{\Omega_{\text{in}}(t)} \frac{-\frac{q^2log(2)}{2} T_j(\mathbf{x})^{\text{qmin}} log_2(T_j(\mathbf{x}))}{\left[G_3^{(\text{in})}(j,t)\right]^2} d\mathbf{x}$$

The $G_i^{(\text{in})}$ functions are defined as:

$$G_1^{(\text{in})}(j,t) = \iiint_{\Omega_{\text{in}}(t)} d\mathbf{x}; \qquad G_2^{(\text{in})}(j,t) = \iiint_{\Omega_{\text{in}}(t)} T_j(\mathbf{x})^{\text{qmax}} d\mathbf{x}$$

$$G_3^{(\text{in})}(j,t) = \iiint_{\Omega_{\text{in}}(t)} T_j(\mathbf{x})^{\text{qmin}} d\mathbf{x}$$

In a similar manner, we establish the expression of $\frac{\partial k_{\text{out}}(\mathbf{x},j,q,t)}{\partial t}$. It can easily be shown that:

$$\iiint_{(\text{out})} \frac{\partial k_{(\text{out})}(\mathbf{x},j,q,t)}{\partial t} = \sum_{i=1}^{3} A_i^{(\text{out})} \int_{\Gamma(t)} H_i^{(\text{out})}(\mathbf{x},j)(\vec{V}.\vec{N})ds \quad (9)$$

with $H_i^{(\text{out})}$ and $A_i^{(\text{out})}$ defined in a symmetric manner to $H_i^{(\text{in})}$ and $A_i^{(\text{in})}$. By replacing (8) and (9) in eq.(7), we can establish the expression of $\frac{\partial E(\Omega,q,j,t)}{\partial t}$:

$$\begin{aligned}\frac{\partial E(\Omega,q,j,t)}{\partial t} = &\int_{\Gamma(t)} (k_{\text{out}} - k_{\text{in}})(\vec{V}.\vec{N})ds + \\ &\sum_{i=1}^{3} A_i^{\text{in}} \int_{\Gamma(t)} H_i^{\text{in}}(\mathbf{x},j)(\vec{V}.\vec{N})ds + \\ &\sum_{i=1}^{3} A_i^{\text{out}} \int_{\Gamma(t)} H_i^{\text{out}}(\mathbf{x},j)(\vec{V}.\vec{N})ds\end{aligned}$$

Given that the speed flow $\vec{v}$ is $\vec{v} = F\vec{N}$, considering only the inner part $E(\Omega,q,j,t)$ of the energy (eq.6), the curve evolution equation would be:

$$\frac{\partial \Gamma(q,j,t)}{\partial t} = F_q(\mathbf{x},j,t)\vec{N}$$

where the flow for a given scale j and order q is:

$$F_q(\mathbf{x},j,t) = k_{\text{in}} - k_{\text{out}} - \sum_{i=1}^{3} A_i^{(\text{in})} H_i^{(\text{in})} - \sum_{i=1}^{3} A_i^{(\text{out})} H_i^{(\text{out})} \quad (10)$$

3.3. Final flow field

Considering the global functional (eq.6), we define the global flow, for all scales and all order of moments:

$$W(\mathbf{x},t) = \sum_{q=-2}^{2} (-s_q \sum_{j=1}^{J} \omega_j F_q(\mathbf{x},j,t))$$

with

$$s_q = \begin{cases} 1 & \text{if } \tau_{\text{in}}(q) >= \tau_{\text{out}}(q) \\ -1 & \text{if } \tau_{\text{in}}(q) < \tau_{\text{out}}(q) \end{cases} \quad (11)$$

The resulting surface evolution equation is expressed as:

$$\frac{\partial \Gamma(t)}{\partial t} = W(\mathbf{x},t)\vec{N} \quad (12)$$

For the numerical implementation, we solve the active contour (12) with a level set method using a standard finite difference scheme. Given the final flow field, the level set equation of our active contour is:

$$\frac{\partial \Phi(x,t)}{\partial t} = W|\nabla\Phi| \quad (13)$$

4. EXPERIMENTAL RESULTS

4.1. Simulated Data

To validate the proposed multifractal active contour under controlled conditions, we generated a simulated $2D$ image (Fig.1). This consists of data generated from a log normal multiplicative cascade ($LNMC$) with $(\mu_{out}, \sigma_{out}) = (0.3, 0.2)$, containing a rectangular area filled up with data from another $LNMC$ with $(\mu_{in}, \sigma_{in}) = (0.6, 0.3)$. This

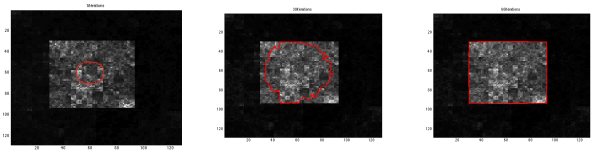

Fig. 1. Synthetic image with the initial curve (top left). Curve evolution at 30 and 60 iterations.

image has been segmented using our algorithm and the parameters $(\tilde{\mu}, \tilde{\sigma})$ have been estimated for each region. Figure 2 shows the behavior of the model parameters during execution. The final estimated parameters are $(\tilde{\mu}_{out}, \tilde{\sigma}_{out}) = (0.298, 0.208)$ and $(\tilde{\mu}_{in}, \tilde{\sigma}_{in}) = (0.602, 0.310)$. Figure 1 shows the result of the segmentation after 60 iterations that took less than 2 minutes on a standard laptop with dual core. The behavior of the global functional (eq.5) as the curve

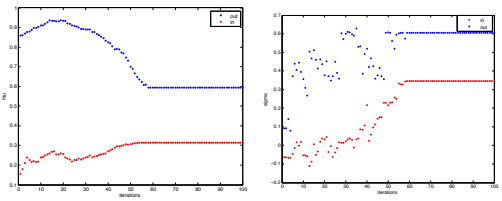

Fig. 2. Evolution of the parameters (μ, σ)

evolves is visualized in Fig. 3. One notices that the functional exhibits a plateau (minimum) when the curve has correctly

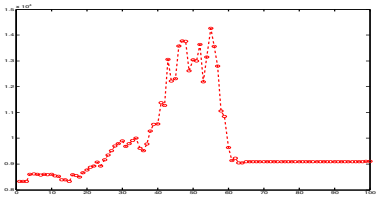

Fig. 3. Evolution of the global functional

delineated the object. The segmentation of the same simulated image with an initial curve partial outside the object leads to similar results after 160 iteration and less than 5 minutes. Convergence has been found more difficult when the initial curve is entirely outside the object. To illustrate the topological changes, a second $2D$ synthetic images with two regions has been simulated. The image contains two objects resulting from the same $LNMC$ within a background from a different $LNMC$. Figure 4 shows the simulated image, the initialisation and segmentation. It can be seen that the algorithm recovers correctly the two objects.

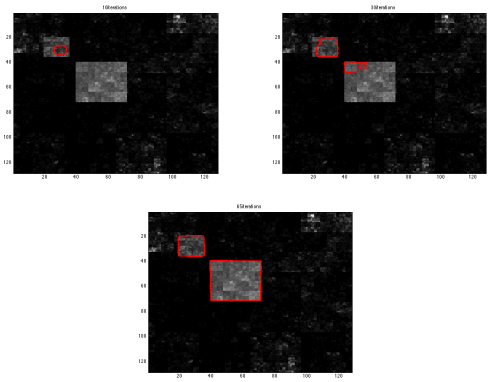

Fig. 4. Synthetic image with two objects. Curve evolution after 10, 30 and 65 iterations.

4.2. Application to real data

This section applies the proposed algorithm to the segmentation of two real high frequency ultrasound skin images having each a melanoma tumor within the dermis tissues. Experiments were conducted using $3D$ high frequency B-mode ultrasound images of in vivo skin tissue. Results are shown for $2D$ slices for display convenience. Images were acquired at 100 MHz with a Dermocup system (Atys Medical France), equipped with a single element focalized 25 MHz $3D$ probe. The proposed multifractal active contour was used to delineate the lesion out from the healthy tissue in the region of interest. Figure 5 shows the results of the segmentation. The multifractal parameters estimated for the melanoma are

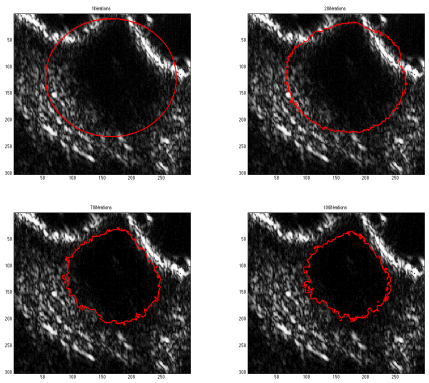

Fig. 5. Evolution of the multifractal active contour on a real ultrasound image to segment a skin lesion (200 iterations).

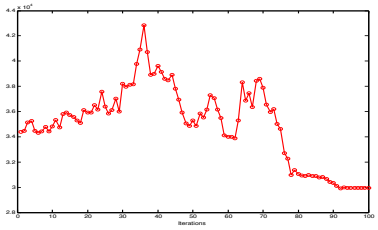

Fig. 6. Evolution of the global functional (eq.5) when segmenting image Fig.5

$(\tilde{\mu}_{out}, \tilde{\sigma}_{out}) = (0.21, 0.48)$ and $(\tilde{\mu}_{in}, \tilde{\sigma}_{in}) = (0.14, 0.32)$. The behavior of the global functional (eq.5) as the curve moves is visualized in Fig. 6. We notice the plateau when the curve achieves the borders of the tumor. The proposed algorithm has also been compared with the state of the art method proposed in [25]. This method considers that the image is a mixture of two Rayleigh components and separates them using an active contour based on the maximum likelihood criterion. The results were obtained after 1000 iterations for the Sarti method and 300 iterations for our proposed multifractal active contour. Results are shown in figure 7. The results show that the shape of the contour obtained by our method is more regular than that of the Sarti method. Convergence has been achieved for the Sarti method after 20 minutes whereas our method converged in 10 minutes.

5. CONCLUSION

Motivated by medical applications, we proposed in this paper an original active contour model based on multifractal properties. This model bridges the gap between statistical active contours based on global and local statics. Using the closed form expression of the exponent function of the proposed stochastic model, we established an energy functional and derived a curve evolution equation using the shape derivation scheme. The corresponding flow is mathematically appealing and was shown to be efficient. A level set implementation was developed. The method was successfully applied to sim-

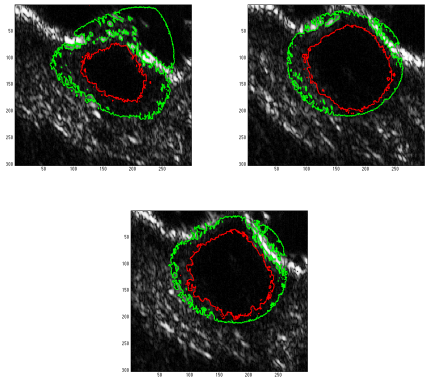

Fig. 7. Comparison of the multifractal active contour (red) and the Sarti [25] contour (green).

ulated log normal cascades and in-vivo high frequency ultrasound skin images. Future work includes the investigation of speeding convergence independently of the initialisation and a thorough characterization of the performance of the segmentation algorithm using clinical data.

REFERENCES

[1] M. Abadi, E. Grandchamp, "Texture features and segmentation based on multifractal approach", in Proc 11th Iberoamerican Congress on Pattern Recognition, 42, Cancun, 14-17 Nov., pp. 297–305, 2006.

[2] D. Boukerroui, "Optimal spatial scale for local region-based active contours", In Proc. ICIP'14, 27-30 Oct., Paris, 2014.

[3] D. Boukerroui, "A local Rayleigh model with spatial scale selection for ultrasound image segmentation", in British Mach. Vis. Conf., R. Bowden, J. Collomosse, and K. Mikolajczyk, Eds., Surrey, Sep. 2012, pp. 8484.

[4] T. Chan, L. Vese, "Active contours without edges. IEEE Trans. on Image Processing", 10, pp.266–277, 2001.

[5] C. Darolti, A. Mertins, C. Bodensteiner, U. G. Hofmann, "Local region descriptors for active contours evolution", IEEE Trans. Image Process., 17(12), pp. 22752288, 2008.

[6] M. Djeddi, A. Ouahabi, H. Batatia, A. Basarab, D. Kouamé, "Discrete wavelet for multifractal texture classification: application to medical ultrasound", IEEE International Conference on Image Processing, Hong Kong, pp. 637-640, 2010.

[7] M. Djeddi, Z. Ouksili, H. Batatia, "A lognormal multiplicative cascade model for multifractal characterization of skin ultrasound images", IEEE International Symposium on Biomedical Imaging, Barcelona, pp.1583-1586, 2012.

[8] S. Ezekiel, "Medical Image Segmentation using multifractal analysis", Proceedings of the Applied Informatics, 378, pp. 220–224, 2003.

[9] S. Guyot, M.C. Peron, E. Delchelle, "Spatial Speckle characterization by Brownian analysis", Physical Review, 70, pp. 46618.1-46618.8, Oct. 2004.

[10] S. Jehan-Besson, M. Barlaud, G. Aubert, "DREAM2S : Deformable regions driven by an Eulerian accurate minimization method for image and video segmentation", International Journal of Computer Vision ,53, pp. 45–70, 2003.

[11] Ji Z., Xia Y., Sun Q., Cao G., Chen Q, "Active contours driven by local likelihood image fitting energy for image segmentation", Information Sciences, Vol. 301, pp. 285-304, April 2015.

[12] M. Jung, G. Peyre, L. D. Cohen", Nonlocal active contours", SIAM J. Imaging Sciences,5(3), pp. 10221054, 2012.

[13] T. Kadir, M. Brady, "Unsupervised non-parametric region segmentation using level sets", in Proc. ICCV, Beijin, 13-16 oct., pp. 12671274, 2003.

[14] S. Lankton, and A. Tannenbaum,"Localizing region-based active contours", IEEE Transactions on Image Processing, 17(11), pp.2029-2039, 2008.

[15] Lecellier, F., Fadili, J., Jehan-Besson, S., Aubert, G., Revenu, M., Saloux, E., "Region-based active contours with exponential family observations", J. Math. Imaging Vis, 36, pp.28–45, 2010.

[16] W. L. Lee, Y. C. Chen, K. S. Hsieh, "Unsupervised segmentation of ultrasonic liver images by multiresolution fractal feature vector", Journal of Clinical Imaging, 29, pp. 235–342, 2005.

[17] C. Li, R. Huang, Z. Ding, J. C. Gatenby, D. N. Metaxas, "A level set method for image segmentation in the presence of intensity inhomogeneities with application to MRI", IEEE Trans. Image Process., vol. 20, no. 7, pp. 20072016, 2011.

[18] J. Liu , H. Zhang", Image segmentation using a local GMM in a variational framework", Journal of Math. Imaging & Vision, pp. 116, 2013.

[19] K. Lu, Q. Wang, N. He, D. Pan, W. Pan, "Nonlocal variational image segmentation models on graphs using the Split Bregman", Journal of Multimedia Systems, Feb. 2014, "http://link.springer.com/content/pdf/10.1007%2Fs00530-013-0351-z.pdf".

[20] A. Mitiche, I. Ben Ayed, "Variational and Level Set Methods in Image Segmentation", Springer topics in signal processing. Springer, 2010.

[21] Noble, J. A., Boukerroui, D., "Ultrasound image segmentation: A survey", IEEE Trans. Medical Imaging, 25, pp. 987-1010, 2006.

[22] M. Pereyra, H. Batatia and S. McLaughlin, "Exploiting information geometry to improve the convergence properties of nonparametric active contours," IEEE Trans. Image Processing, to appear.

[23] G. Peyre, J. M. Fadili , J. Rabin, "Wasserstein Active Contours", in Proc. of ICIP12, Orlando, 30 Sep. - 3 Oct., 2012.

[24] J. Piovano, M. Rousson, T. Papadopoulo, "Efficient segmentation of piecewise smooth images. in Scale Space and Variational Methods in Computer Vision", Lecture Notes in Computer Science, F. Sgallari, A. Murli, and N. Paragios, Eds. Springer Berlin Heidelberg, vol. 4485, pp. 709720, 2007.

[25] Sarti, A., Corsi, C., Mazzini, E., Lamberti, C., "Maximum likelihood segmentation of ultrasound images with rayleigh distribution", IEEE Trans. UFFC , 52, pp.947–960, 2005.

[26] L. Wang, C. Li, Q. Sun, D. Xia, C.Y. Kao, "Active contours driven by local and global intensity fitting energy with application to brain MR image segmentation", Int. Journal of Comput. Med. Imag. Graph., 33(7), pp. 520531, 2009.

[27] H. Wang , T.Z. Huang , Z. Xu , Y. Wang, "An active contour model and its algorithms with local and global Gaussian distribution fitting energies", Information Sciences, vol. 263, pp. 43 - 59, 2014.

[28] H. Wendt, P. Abry, S. Jaffard, H. Ji, Z. Shen,"Wavelet leader multifractal analysis for texture classification", inProc. IEEE ICIP, pp.3829-3832, 2009.

[29] H. Zhang , Y. Chen , J. Shi, "Nonparametric image segmentation using Renyi's statistical dependence measure", Journal of Math. Imaging & Vision, vol. 44(3), pp. 330340, 2012.

[30] X. Zhuang, Q. Meng, "Local fuzzy fractal dimension and its application in medical image processing", Artificial Intelligence in Medicine, 32, pp. 29-36, 2004.